

On Bouncing Oil Drops

A Thesis
Presented to
The Division of Mathematics and Natural Sciences
Reed College

In Partial Fulfillment
of the Requirements for the Degree
Bachelor of Arts

Miguel B. Conner

May 2015

Approved for the Division
(Physics)

Daniel Borrero

Blog

This is the portion of the thesis that I will update regularly with rough notes, lit reviews, results, etc. some of which will be worked in to the real document after some polishing.

0.1 To Do

- Ch 2: CITE conversation with John Bush. Miguel 4/22/15
- Write Ch 1, and Conclusion. Miguel 4/6/15
- Learn de Broglie's interpretation of QM. Miguel 11/6/14

0.1.1 Done

- Write Intro, Ch2, Ch3. Miguel 4/20/15
- Analyze data. Miguel 4/6/15
- Take data. Miguel 12/2/14
- Figure out citations. 4/6/15
- Set up Accelerometer (Finally–ugh). Miguel 2/20/15
- Get New Silicone Oil. Miguel 1/10/15
- Send copy of Lit Rev to Daniel to proofread. 12/23/14
- Find walking regime. Miguel 11/20/14
- Order Accelerometer. Miguel 11/6/14
- Learn Basics of Bohmian Mechanics. Miguel 10/28/14
- Make tray. Miguel 10/20/14
- Sort out camera situation. Miguel 10/20/14
- Obtain flashdrives. Miguel 9/30/14
- Learn how to use the new L^AT_EX and Github setup. Miguel 9/30/14

0.2 Literature Review

(Important: Particle-wave association on a fluid interface (Protiere 2006)).

In 2005, Yves Couder showed that bouncing oil drops on vertically vibrating fluid bath exhibited properties analogous to the paradoxical properties seen only at the quantum scale (CITE: Dynamical phenomena: Walking and orbiting droplets?). Couder, John Bush, and others have shown that this system can reproduce double-slit single-particle interference, orbiting, tunneling, quantized orbits, spin, and more. The trajectory of the droplet can be modeled mathematically, and the dynamics of the walker have similarities to de Broglie's theory of quantum mechanics (CITE: Bush 2015).

The literature review will begin with a description of Faraday waves and the basic dynamics of a bouncing droplet and a walking droplet. Then we will describe in detail a few of the important quantum-like properites of this system.

0.2.1 Walking Droplets

It was Couder who then showed that an oil droplet could live for much longer. Long lifetimes meant that the focus could shift from how the droplet bounced (short time scale) to its interactions with other droplets and its motion (longer time scale).

Every time the droplet impacts the bath, it creates a radial traveling wave. If the bouncing droplet impacts the wavefield in such a way that it receives a lateral force from the slope of the wave, then it will be pushed to the side slightly. The next time the droplet makes contact with the bath, it will again make contact with a slope, and be pushed to the side. This propels the bouncing droplet, causing it to "walk" across the surface of the bath. These "walkers" turned out to have particularly interesting behaviours. Indeed, in 2006 Yves Couder and Emmanuel Fort showed that these droplets mimicked the behavior of electrons in the hallmark experiment of quantum weirdness: the double slit experiment. This was the first time that microscopic scale behavior had ever been seen at a macroscopic level, and it sparked interest in the experiment.

0.2.2 Bound States

A bouncing droplet creates a damped wave that depends on the driving acceleration (γ_m/g) CITE: Protiere 2005. A periodic damped wave allows for two bouncers to form a "bound state". Starting far away from one another, the two droplets drift towards one another until a fixed distance d_0^{bd} . Increasing driving acceleration will decrease the value of d_0^{bd} . These bound bouncers form triangular lattices, and their periodicity is highly sensitive to the mass of the droplet. (LOOK AT EDDI ET ALL 2008).

Walkers can also form bound states. Two walkers of the same size that are approaching one another can form an orbit around their center of mass. Between the two droplets is the fixed distance d_n^{orb} given by

$$d_n^{orb} = (n - \epsilon_0)\lambda_F \quad (1)$$

where ϵ_0 is a fixed distance which is the same for all orbitals of these walkers (usually in the range $0.15 < \epsilon_0 < 0.25$ depending on droplet diameter), and $n = 1, 2, 3\dots$ for drops that are in phase or $n = 1/2, 3/2, 5/2\dots$ for drops out of phase. Orbiting periods are approximately proportional to d_n^{orb} , which ends up meaning that the velocity of the orbiting walkers is a little less than the velocity of a free walker CITE: Protiere 2006. Orbiting of different sized droplets can also arise.

0.2.3 Scattering States

Two identical walkers headed towards each other can form fixed orbits, or they can scatter. The droplets are deflected through their wavefields (they never actually make contact with one another)

0.2.4 Motion in a Confined Geomtry

By tracking the droplet as it bounces around the tray over a period of time, one can look at the overall statistical behavior of the droplet. Two experiments tracked walkers in an experimental coral (Harris and Bush, 2013, Harris et al. 2013) in the high-memory, chaotic motion regime. A histogram of the statistical data shows that the "probability of finding a walker at a given point in the corral is roughly prescribed by the amplitude of the Faraday wave mode of the cavity at the prescribed forcing frequency."

Quantum corral experiments performed by Crommie et al. (Crommie et al. 1993 a b) present similar findings. In the experiment, electrons were confined in a Cu(III) substrate using barriers of iron adatoms. Using tunneling spectroscopy, the electrons were found to have a specific resonances depending on the corral shape. As in the case of Harris' circular corral experiment where the corral and the Faraday wavelength, λ_F , dictate the wavelike statistical pattern, in the quantum experiment the corral and the *de Broglie* wavelength, λ_{dB} , dictate the form of the wavelike statistical pattern.

0.2.5 Walker Trajectories

In the regime of walkers we have $R_e \sim 20$, $B_0 \sim 0.1$, and $W_e \sim 0.1$. For the millimeric walkers, the dominant force comes from impact of the curvature of the surface. Gilet and Bush (2009: Chaotic bouncing of a drop on a soap film, and the fluid trampoline: droplets bouncing on a soap film) show that the surface of the vibrating oil can be modeled with a soap film, where the soap film acts like a linear spring.

As the oil bath is forced up and down, a tiny droplet of oil will "walk" across the surface. Moláček and Bush have developed an equation of a droplet that describes the trajectory of the walking droplet, ignoring the vertical dynamics by time averaging them out (cite: J. Moláček and J. W. M. Bush, "Drops walking on a vibrating bath: towards a hydrodynamic pilot-wave theory" J. FluidMech. 727, 612-647 (2013).).

The trajectory of the walking droplet of mass m at position $\mathbf{x}(t) = (x(t), y(t))$ is given by

$$m\ddot{\mathbf{x}} + D\dot{\mathbf{x}} = -mg\nabla h(\mathbf{x}, t) \quad (2)$$

where D describes the drag coefficient and $h(\mathbf{x}, t)$ describes the shape of the wavefield. Thus the second term describes the time averaged drag from both the flight and the impact of the droplet (as usual, depends on the velocity), and the third term describes the propulsive wave force resulting from drops landing on the inclined wave surface.

The wavefield is quite complicated because it depends on the memory. For a single impact of a droplet, Oza et al. argue the surface wave can be approximated with an integral of a monochromatic radial Bessel function of the first kind

$$h(\mathbf{x}, t) = \frac{F}{T_F} \int_{-\infty}^t J_0\left(\frac{k_F|\mathbf{x}(t) - \mathbf{x}(s)|}{|\mathbf{x}(t) - \mathbf{x}(s)|}\right) (\mathbf{x}(t) - \mathbf{x}(s)) e^{-(t-s)/(T_F M_e)} ds \quad (3)$$

with F giving the wave force coefficient (estimated in the above source), T_F describing the Faraday period, and k_F describing the Faraday wave number determined by the Faraday wavelength $\lambda_F = 2/k_F$ (integral from A. U. Oza, D. M. Harris, R. R. Rosales, and J. W. M. Bush, "Pilot-wave dynamics in a rotating frame: on the emergence of orbital quantization" J. Fluid Mech. 744, 404-429 (2014).). (Faraday was a popular guy.) Finally, that last term M_e is the nondimensional memory parameter $M_e = T_d/[T_F(1 - \gamma/\gamma_F)]$ (with T_d being the unforced decay time).

0.3 Bohmian Mechanics

0.3.1 Formalism

The Schrödinger Equation and ψ

We begin with the Schrödinger equation

$$i\hbar \frac{\partial}{\partial t} \psi = \hat{H} \psi \quad (4)$$

where \hat{H} is the Hamiltonian and ψ is the wavefunction. The Hamiltonian can be expanded (assuming there is no electric field) to give

$$i\hbar \frac{\partial}{\partial t} \psi(\mathbf{x}, t) = \left[\frac{-\hbar^2}{2m} \nabla^2 + V(\mathbf{x}, t) \right] \psi(\mathbf{x}, t) \quad (5)$$

where $V(\mathbf{x}, t)$ is the potential energy of the system. The solution ψ is of the form:

$$\psi(\mathbf{x}, t) = R(\mathbf{x}, t) e^{iS(\mathbf{x}, t)/\hbar} \quad (6)$$

where S and R are real. Plugging in our equation for ψ into the Schrödinger equation (Eq. (5)) will produce two separate equations: one giving the time derivative of R and the second giving the time derivative of S . From these equations, a Hamilton-Jacobi equation can be written for a quantum system. Let's begin by computing the left hand side of Eq. (5) in terms of R and S .

$$\begin{aligned}
i\hbar \frac{\partial}{\partial t} \psi(\mathbf{x}, t) &= i\hbar \left(\frac{\partial R}{\partial t} e^{iS/\hbar} + R \frac{i}{\hbar} \frac{\partial S}{\partial t} e^{iS/\hbar} \right) \\
&= i\hbar \left(\frac{1}{R} \frac{\partial R}{\partial t} + \frac{i}{\hbar} \frac{\partial S}{\partial t} \right) \psi(\mathbf{x}, t) \\
&= \left(i\hbar \frac{1}{R} \frac{\partial R}{\partial t} - \frac{\partial S}{\partial t} \right) \psi(\mathbf{x}, t)
\end{aligned}$$

Let's leave that alone for a little bit, while we focus on the right hand side of Eq. (5). Since it's a little more complicated, we will start with one term of the right hand side:

$$\begin{aligned}
\nabla^2 \psi(\mathbf{x}, t) &= e^{iS/\hbar} \nabla^2 R + \left(\frac{i}{\hbar} \right)^2 (\nabla S)^2 R e^{iS/\hbar} + \left(\frac{i}{\hbar} \right) R e^{iS/\hbar} (\nabla^2 S) + \left(\frac{2i}{\hbar} \right) (\nabla R \cdot \nabla S) R e^{iS/\hbar} \\
&= \left(\frac{\nabla^2 R}{R} - \left(\frac{\nabla S}{\hbar} \right)^2 + \left(\frac{i \nabla^2 S}{\hbar} \right) + 2i \left(\frac{\nabla R \cdot \nabla S}{\hbar} \right) \right) \psi(\mathbf{x}, t)
\end{aligned}$$

Now the hard part is done, and we can say that the right hand side of Eq. (5) is given by

$$\left[\frac{-\hbar^2}{2m} \nabla^2 + V(\mathbf{x}, t) \right] \psi(\mathbf{x}, t) = \left[-\frac{\hbar^2 \nabla^2 R}{2mR} + \left(\frac{(\nabla S)^2}{2m} \right) - i\hbar \left(\frac{\nabla^2 S}{2m} \right) - i\hbar \left(\frac{\nabla R \cdot \nabla S}{m} \right) + V(\mathbf{x}, t) \right] \psi(\mathbf{x}, t)$$

Ok, now that we've got that done, the next part will be super easy. Starting with Schrodinger's equation and plugging in left and right hand sides we calculated seperately.

$$\begin{aligned}
i\hbar \frac{\partial}{\partial t} \psi(\mathbf{x}, t) &= \left[\frac{-\hbar^2}{2m} \nabla^2 + V(\mathbf{x}, t) \right] \psi(\mathbf{x}, t) \\
\left(i\hbar \frac{1}{R} \frac{\partial R}{\partial t} - \frac{\partial S}{\partial t} \right) \psi(\mathbf{x}, t) &= \left[-\frac{\hbar^2 \nabla^2 R}{2mR} + \left(\frac{(\nabla S)^2}{2m} \right) - i\hbar \left(\frac{\nabla^2 S}{2m} \right) - i\hbar \left(\frac{\nabla R \cdot \nabla S}{m} \right) + V(\mathbf{x}, t) \right] \psi(\mathbf{x}, t)
\end{aligned}$$

Now we can divide out ψ from both sides

$$i\hbar \frac{1}{R} \frac{\partial R}{\partial t} - \frac{\partial S}{\partial t} = -\frac{\hbar^2 \nabla^2 R}{2mR} + \left(\frac{(\nabla S)^2}{2m} \right) - i\hbar \left(\frac{\nabla^2 S}{2m} \right) - i\hbar \left(\frac{\nabla R \cdot \nabla S}{m} \right) + V(\mathbf{x}, t)$$

and group the imaginary numbers on the left side and the real numbers on the right side

$$i\hbar \frac{1}{R} \frac{\partial R}{\partial t} + i\hbar \left(\frac{\nabla^2 S}{2m} \right) + i\hbar \left(\frac{\nabla R \cdot \nabla S}{m} \right) = \frac{\partial S}{\partial t} - \frac{\hbar^2 \nabla^2 R}{2mR} + \left(\frac{(\nabla S)^2}{2m} \right) + V(\mathbf{x}, t)$$

Recall that both S and R are real. Note that the only way for all of the imaginary terms to equal all of the real terms is if they both equaled zero.

$$i\hbar \left(\frac{1}{R} \frac{\partial R}{\partial t} + \frac{\nabla^2 S}{2m} + \frac{\nabla R \cdot \nabla S}{m} \right) = \left(\frac{\partial S}{\partial t} - \frac{\hbar^2}{2m} \frac{\nabla^2 R}{R} + \frac{(\nabla S)^2}{2m} + V(\mathbf{x}, t) \right) = 0$$

This then gives us two separate equations, one for the time derivative of R and another for the time derivative of S .

$$\frac{\partial R}{\partial t} = -\frac{R}{2m} \left(\frac{\nabla^2 S}{m} - 2\nabla R \cdot \nabla S \right) \quad (7)$$

$$\frac{\partial S}{\partial t} = \frac{\hbar^2}{2m} \frac{\nabla^2 R}{R} - \frac{(\nabla S)^2}{2m} - V(\mathbf{x}, t) \quad (8)$$

What does this do for us? Both equations will provide helpful descriptions of our system.

The Quantum Potential

We can rewrite Eq. (8) in a provocative way

$$-\frac{\partial S}{\partial t} = \frac{(\nabla S)^2}{2m} + V(\mathbf{x}, t) + \frac{\hbar^2}{2m} \frac{\nabla^2 R}{R} \quad (9)$$

which should look suspiciously familiar. If I were to tell you that ∇S had units of momentum and $\partial S/\partial t$ units of energy, then this equation would look a lot like a Hamiltonian! The first term takes care of the kinetic energy, the second is the potential energy term, but we have this mysterious third term which we haven't ever encountered in classical mechanics. If we define this term as our "quantum potential"

$$U(\mathbf{x}) = \frac{\hbar^2}{2m} \frac{\nabla^2 R}{R} = \frac{\hbar^2}{4m} \left[\frac{1}{2} \frac{\nabla^2 P}{P} - \frac{(\nabla P)^2}{P^2} \right] \quad (10)$$

then we really *can* think of Eq. (9) as a Hamiltonian with an extra potential term thrown in to make it "quantum." Note that in cases where \hbar is much smaller than the rest of the terms (i.e. not the quantum realm), then this quantum potential term goes away, and we are left with the regular Hamilton equation from classical mechanics.

Recall that when writing a Hamiltonian, the potential terms govern the forces on the particle. For a conservative system, the force is given by $\mathbf{F}(\mathbf{x}) = -\partial U/\partial \mathbf{x}$. If we include a quantum mechanical potential in our Hamiltonian, then this potential must cause a force on the particle in addition to the one supplied by the $V(x)$ term.

Continuity Equation

Plugging in the probability density $P(\mathbf{x}, t) = R^2(\mathbf{x}, t)$ into Eq. (7) also gives us something quite interesting.

MATH?

which we can finally express as

$$\frac{\partial P}{\partial t} + \nabla \cdot \left(P \frac{\nabla S}{m} \right) \quad (11)$$

In describing the quantum potential term it was mentioned that ∇S can be thought of as momentum, so then from our classical relationship between momen-

tum and velocity $\mathbf{v}(\mathbf{x}, t) = \nabla S/m$ can be thought of as velocity. Then by defining the probability current as $j(\mathbf{x}, t) = P\nabla S/m$ then we recover

$$\frac{\partial P}{\partial t} + \nabla \cdot j(\mathbf{x}, t) \quad (12)$$

known as the continuity equation! This tells us that P is conserved over time.

Finding R and S

Introduction

“While the founding fathers agonized over the question ‘particle’ or ‘wave’, de Broglie in 1925 proposed the obvious answer ‘particle’ and ‘wave’... [t]his idea seems to me so natural and simple, to resolve the wave-particle dilemma in such a clear and ordinary way, that it is a great mystery to me that it was so generally ignored.” -J. S. Bell

Quantum Mechanics is perhaps one of the most counter-intuitive scientific theories in the history of the scientific method. At the atomic level, where quantum effects dominate, the laws that seem to govern our everyday world are thrown out of the window. Determinism, the idea that every effect has a cause, was replaced with the idea that every action is probabilistic. The Copenhagen interpretation of quantum mechanics represents the most common interpretation. Quantum Mechanics has stuck around because it fits well with experiment, which is the only true test of a theory’s validity.

In 2005, Couder et al. showed that oil drops bouncing on vertically vibrated fluid bath exhibit properties analogous to the paradoxical properties previously seen only at the quantum scale [1]. The system operates at the macro-scale, meaning that it is governed by the more “intuitive” physical laws (i.e. not quantum), but still behaves *like* a quantum system. With that said, the experiment is a visualization of some fundamental quantum phenomena, whether or not the atomic processes actually operate like the macroscopic ones. For example, in quantum mechanics, one can never know the position and the velocity of a particle, simply because it can never have a perfectly defined position and velocity. In this experiment however, the “particle” can be easily seen at all times, so position and velocity can be easily tracked.

The behavior of the droplet system seems to be in line with a theory of quantum mechanics proposed by Louis de Broglie in 1924(?): pilot-wave theory. The main concept is that a guiding wave pushes a particle. The theory was extended by David Bohm in 1952 [2] [3], but never caught on because it gained “realism” (the idea that a particle is well defined at all times) at the expense of “locality” (the universal speed limit: nothing can travel faster than the speed of light), a trade that is generally considered unfavorable to physicists.¹ The theory is also undeveloped, having remained relatively obscure for the past couple of decades. Experiments have not suggested one theory over any other, for the most part the predictions are the same. As a result, things have stayed the way they have been.

¹The Copenhagen interpretation of quantum mechanics, by the way, is non-realist but local.

My interest alternative theories of quantum mechanics is what drew me to this experiment. After learning the standard way in class, I thought it would be interesting to explore a more obscure subject. Also, this quantum analog gives me a chance to perform an experimental investigation. Up till now, I've mostly just described the implications of the system, but now I will explain how the system works.

0.3.2 Bouncing Droplets

Though it had been observed for at least a century, the phenomena of droplets bouncing on a fluid bath was first explained by Jearl Walker in 1978 [4]. The investigations began with a simple droplet of water falling onto a bath of water, and remaining just a second too long before coalescence.² Walker then discovered that by adding detergent to the water and then vibrating the bath he could extend the lifetime of the droplets from fractions of a second to several minutes. Because these droplets are bouncing at frequencies of around 50 Hz (50 bounces per second) and the droplets are very small to begin with (with a diameter of a millimeter or less), it can be difficult to observe even the main mechanisms that drive the behavior. A key insight by Walker was that by flashing a strobe light at a frequency slightly slower than the rate of vibration of the bath, he could observe the droplet bouncing as if in slow motion.

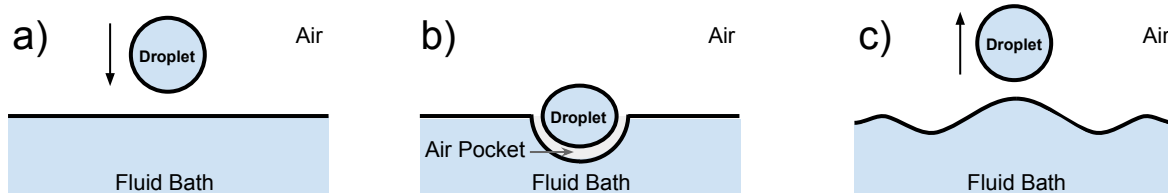


Figure 1: A depiction of a droplet bouncing on a bath of the same fluid. (a) A droplet falls onto a fluid bath. (b) A film of air gets trapped underneath the droplet. (c) The droplet bounces back up off the cushion of air leaving behind waves that propagate radially.

Walker found that a trapped film of air kept the droplet and the bath from touching, as shown in Fig. 3. That is, the droplet is bouncing on a layer of air that's struggling to get out of the way but because the bounce happens so quickly, the fluid droplet and the fluid bath never touch. Walker concluded that the leakage rate of this trapped pocket of air depends on three factors: the surface tension of the fluid in the bath, the viscosity of the droplet and the fluid bath, and the viscosity of the air. The bath must be of uniform surface tension and free from particulate matter floating atop the bath, since both will lead to coalescence. Higher viscosity fluids translate to longer droplet lifetimes, since more viscous fluids keep air from escaping the pocket. Finally, adjusting the frequency and the amplitudes of the vibrations also affects droplet lifetime.³

²It is often reported that this occurs in coffeemakers, as the coffee drips into the pot.

³Reedie Andrew Case ('92) wrote his thesis "Oil on Troubled Water: The Extension of Floating Drop Lifetimes Due to Interface Vibration" where he looked at droplet lifetime by the frequency of

More recent research suggests that a droplet fluid like silicone oil could bounce indefinitely off a vibrating bath [5]. The long lifetime occurs not only because silicone oil has a high viscosity, but also because it has a *low* surface tension. A low surface tension is beneficial because it makes the oil bath relatively immune to surfactants (surface acting agents) or contamination which would otherwise make the surface tension nonuniform, and thus create a coalescence event.

0.3.3 Faraday Waves

For a vertically vibrated fluid bath, controlling the amplitude and the frequency of the motion will affect the behavior of the fluid. Depending on a variety of factors (size of bath, fluid in bath, etc.) each system has a specific amplitude (given a specific frequency), which if surpassed, will produce standing surface waves called Faraday waves [6].⁴ ⁵ A vibrating bath below this critical amplitude, also known as the Faraday instability, will be flat and motionless. A bath with a amplitude greater than the Faraday threshold will have a turbulent surface with ripples and waves. An example of Faraday waves is shown in Fig. 2. Adjusting the frequency above the Faraday threshold will change the size and shape of the Faraday waves. Note that Faraday waves can be created either by increasing amplitude to a critical level, or increasing frequency to a critical level.



Figure 2: A picture of Faraday waves in a dish of water at 80 Hz.

vibration.

⁴Faraday waves weren't actually discovered by Michael Faraday, they were originally discovered by X.

⁵Another Reed thesis, this one titled "Good Vibrations: A Visual Exploration of Faraday Waves" by Alison Saunders, compares mathematical formulation to experimental results.

0.3.4 Walking Droplets

A bouncing droplet will bounce differently depending on the frequency and amplitude of the vertical vibrations. If the parameters are set just a hair below the Faraday instability, then a very curious motion arises: the droplet seems to “walk” across the surface of the oil. The droplet is being pushed by its own ripples, a dual effort in which neither can exist without the other. In essence, the walker is both a particle and a wave; a conjunction which has only ever been seen at the quantum scale.

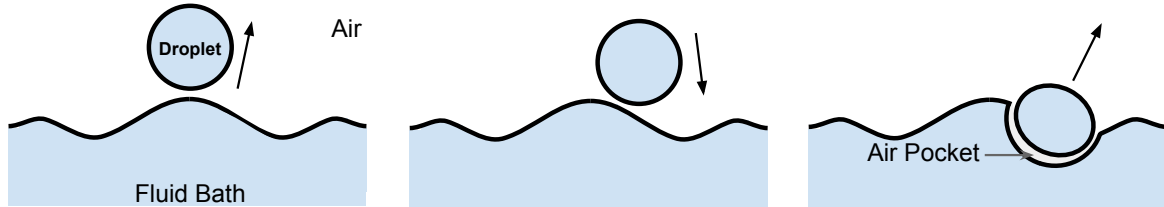


Figure 3: A depiction of a droplet walking across a bath of the same fluid.

0.3.5 Road Map

Recently, two main groups have been investigating the properties of this unique system. A group at Laboratoire Matière et Systèmes Complexes (MSC) in Paris, France, headed by Yves Couder was the first to uncover some of the inherently “quantum”-like behavior of bouncing droplets, in 2005 [1]. Since 2010 John Bush’s group at MIT have been adding to the literature by creating a mathematical model, and performing their own investigations of the walker system. Couder, Bush, and others have shown that this system can reproduce double-slit single-particle interference, orbiting, tunneling, quantized orbits, spin, and many more “quantum”-like effects.

The thesis documents an experimental investigation into a “tunneling” behavior of this bouncing droplet system. While only one other study really looks at this aspect [7], it falls short of completely examining the tunneling behavior, focusing on barrier width and not examining barrier height. I hope to add the body of work in this subfield by studying how barrier height affects probability of tunneling.

This thesis is divided into three main chapters. **Chapter 1** gives a background of the hydrodynamic quantum analogs along with a brief survey of the relevant literature. In **Chapter 2**, I lay out the experimental design and explain the setup and the data taking procedures. Finally, the results and conclusions are presented in **Chapter 3**.

Chapter 1

Pilot-Wave Hydrodynamics

In this chapter I will present a brief survey of the literature describing the hydrodynamic quantum analog, and discuss in more detail the particular tunneling experiments relevant to my investigation. Because the system was discovered in 2005, most of the literature examining this topic was written within the last ten years and is constantly advancing.

1.1 Oil Droplet System

Consider a fluid of density ρ , viscosity ν , and surface tension σ in a bath of depth H . This fluid bath is driven vertically at an amplitude A_0 at frequency $f = \omega/2\pi$. By defining $\gamma = A_0\omega^2$, the effective gravity in the frame of reference of the bath is $g + \gamma \sin(\omega t)$. The surface of oil in the shaking tray remains quiescent for lower values of γ . However, if one continues to increase γ (by increasing A_0 or f), one will eventually witness the appearance of standing surface waves called Faraday waves. We define the threshold at which these waves appear as the **Faraday threshold** γ_F , the value of which changes depending on the size and shape of the tray, the amount of fluid in the tray, and the properties of the fluid.

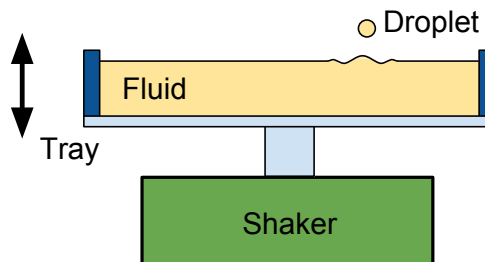


Figure 1.1: A droplet bounces on a vertically vibrating fluid bath. The tray vibrates with an amplitude A_0 at frequency f .

If we take a toothpick and break the surface of the vibrating oil bath, we form a droplet of oil that will remain bouncing for hours as shown in Fig. 1.1. The droplet bounces on a pocket of air, trapped beneath the droplet and the bath [4]. As the

oil droplet of diameter D bounces, it creates radially traveling waves that propagate outwards in an otherwise placid surface. The droplet will continue bouncing for a specific range of values of γ . For a small γ , the forcing is not enough to sustain the droplet, and it quickly coalesces. Increasing γ will yield changes to the droplet's dynamics until $\gamma > \gamma_F$, where the droplet bounces on the standing Faraday waves and can jump out of the tray. We are interested in studying the region below the appearance of Faraday waves but above the region of coalescence. The range of the various parameters which allow for the existence of the bouncing droplet are outlined in Table 1.1.

Table 1.1: Approximate limits for bouncing drop behavior. The value $g = 9.81\text{ms}^{-2}$ is the standard acceleration due to gravity.

| Parameter | Lower Limit | Upper Limit |
|----------------------------------------------------|-------------|-------------------------|
| Viscosity ν (cSt) | 10 | 100 |
| Bath Depth H (mm) | 4 | 10 |
| Frequency f (Hz) | 20 | 150 |
| Amplitude A_0 (mm) | 0.1 | 1 |
| Drop Diameter D (mm) | 0.6 | 1.0 |
| Forcing Acceleration γ (ms^{-2}) | 0.5g | $\gamma_F \approx 4.2g$ |

1.1.1 Faraday Waves

At a forcing $\gamma = \gamma_F$ we see the appearance of standing surface waves known as Faraday waves. These waves have frequency $f_F = f/2$ and a angular frequency $\omega_F = 2\pi f_F = \pi f$. For a fluid bath of density ρ , surface tension σ , and height H , the standing wave and water dispersion relation can be used to find the wavelengths of standing waves at the Faraday threshold:

$$\omega_F^2 = \left(gk_F + \frac{\sigma k_F^3}{\rho} \right) \tanh(k_F H), \quad (1.1)$$

which relates the angular Faraday frequency ω_F to the Faraday wavenumber k_F , where g is the gravitational constant [8]. From the wavenumber, we can calculate the wavelength λ_F of the Faraday waves by the relation $\lambda_F = 2\pi/k_F$. Though we are interested in investigating the region $\gamma < \gamma_F$ for which there are no standing surface waves, Eq. (1.1) provides an estimate to the wavelength and frequency of the localized waves surrounding the droplet for the bouncing behavior.

1.1.2 Vibration Number

In an experiment, one usually pours in a specific volume of oil in the tray, fixing the values of ν , σ , and H . One is then left with the option to adjust γ which produces

a range of droplet motions, including a slew of different stationary bouncing modes and linear or chaotic “walking” trajectories (which are discussed later). To visualize the various bouncing behaviors, we use the vibration number V_i , which takes into account many of the parameters of the experiment [9]. The vibration number is the ratio of the forcing frequency and the drop’s natural oscillation frequency:

$$V_i = \frac{\omega}{\omega_D} \quad (1.2)$$

where ω_D represents the oscillation frequency of a fluid droplet. In other words, it represents ...!!! The oscillation frequency of a fluid droplet is defined as:

$$\omega_D = 2\sqrt{\frac{2\sigma}{\rho D^3}}, \quad (1.3)$$

with surface tension σ , density ρ , and diameter of the droplet D [10]. Combining Eqs. 1.2–1.3 we arrive at:

$$V_i = \frac{\omega}{2} \sqrt{\frac{\rho D^3}{2\sigma}}, \quad (1.4)$$

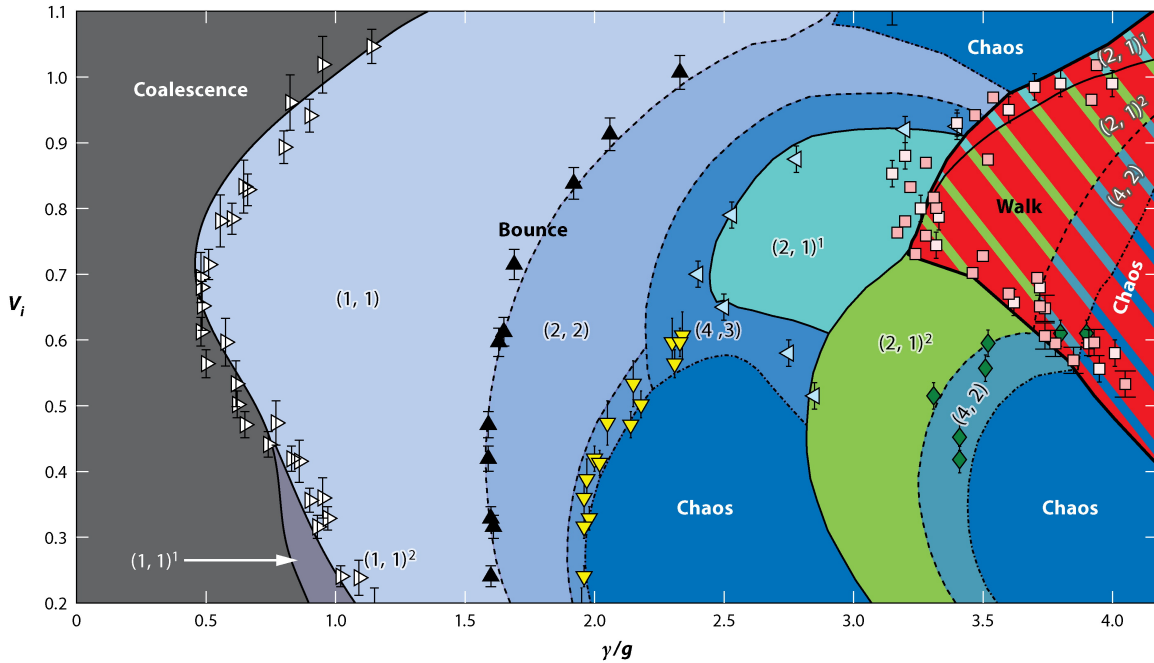
a dimensionless parameter that captures the fluid’s surface tension σ and density ρ , the tray’s vibration ω , and the droplet’s diameter D . Depending on the vibration number V_i and the driving frequency γ/g the droplets switch between different bouncing states as shown in Fig. 1.2. If we hold the fluid and the frequency constant (σ , ρ , and ω), then Eq. (1.4) says we can think of increasing V_i as and increasing droplet diameter D .

The various modes seen in Fig. 1.2 can be described by (m,n) , where n is the number to times the droplet contacts the surface over a time span m/f . For example, in the $(1, 1)$ “bounce” mode, the droplet hits the oil bath once per up-and-down motion of the tray. In the $(2, 2)$ mode, the drop makes two bounces of differing heights for two driving periods. The “chaos” regimes indicate that the bouncing of the droplet is chaotic, and it does not seem to exhibit a periodic bouncing motion. The “walk” regime describes a very particular kind of behavior in which the droplet moves forward as it bounces, seemingly walking across the surface. Like bouncing, walking also comes either the $(2, 1)$, $(4, 2)$, or the chaos mode. Finally, the “coalescence” region demarcates the values for which the droplet coalesces with the bath.

The droplet map shown in Fig. 1.2 provides a valuable starting place for an experiment since it outlines the many possible states of the system, and where we can expect to find particular behaviors. We will now narrow our focus to only the walking regime, for which a variety of fascinating interactions emerge.

1.1.3 Walking

A walking droplet is a very specific type of bouncing droplet. As the droplet bounces vertically on the vibrating fluid bath, the interaction of its previous waves give it a slight horizontal motion with every bounce. Thus, for every bounce, the droplet follows a parabolic trajectory. But because these droplets are bouncing at 40 times



A Bush JWM. 2015.
R Annu. Rev. Fluid Mech. 47:269–92

Figure 1.2: The different bouncing regimes for the oil drops of 20 cSt silicone oil at $f = \omega/2\pi = 80$ Hz, characterized by the non-dimensionalized forcing frequency γ/g and the vibration number V_i . The solid colors represent the modes predicted by a theoretical model [9], and the various points represent experimentally measured limits. The parameters $(m, n)^i$ describe a droplet that bounces n times in m forcing periods, where i distinguishes modes with different mechanical energy. The Faraday threshold is $\gamma_F = 4.2$. This diagram was taken from [11].

per second (or more) and the parabolic motion is periodic, the vertical oscillations are difficult to see. The apparent behavior that emerges is that of the droplet moving in a straight line along the surface of the fluid bath.

The horizontal component of the walker is due to the droplet landing slightly off center of the radial wave it produced in the previous bounce, shown in Fig. 1.3. At such close proximity to the Faraday threshold, the waves surrounding the droplet are not just regular ripples, but rather are like localized Faraday waves because they are sustained by the vibrations. The kinetic energy from the falling droplet is enough to perturb the unstable surface such that the waves are sustained for a longer period of time. As these waves interfere with one another they create an overall wave field that guides the droplet. This overall wave field is referred to as the **guiding wave** or the **pilot wave**. The **walker** is defined as both the droplet and its guiding wave, since they are mutually dependent. The unique combination of the two components results in novel interactions like bound states or scattering states.

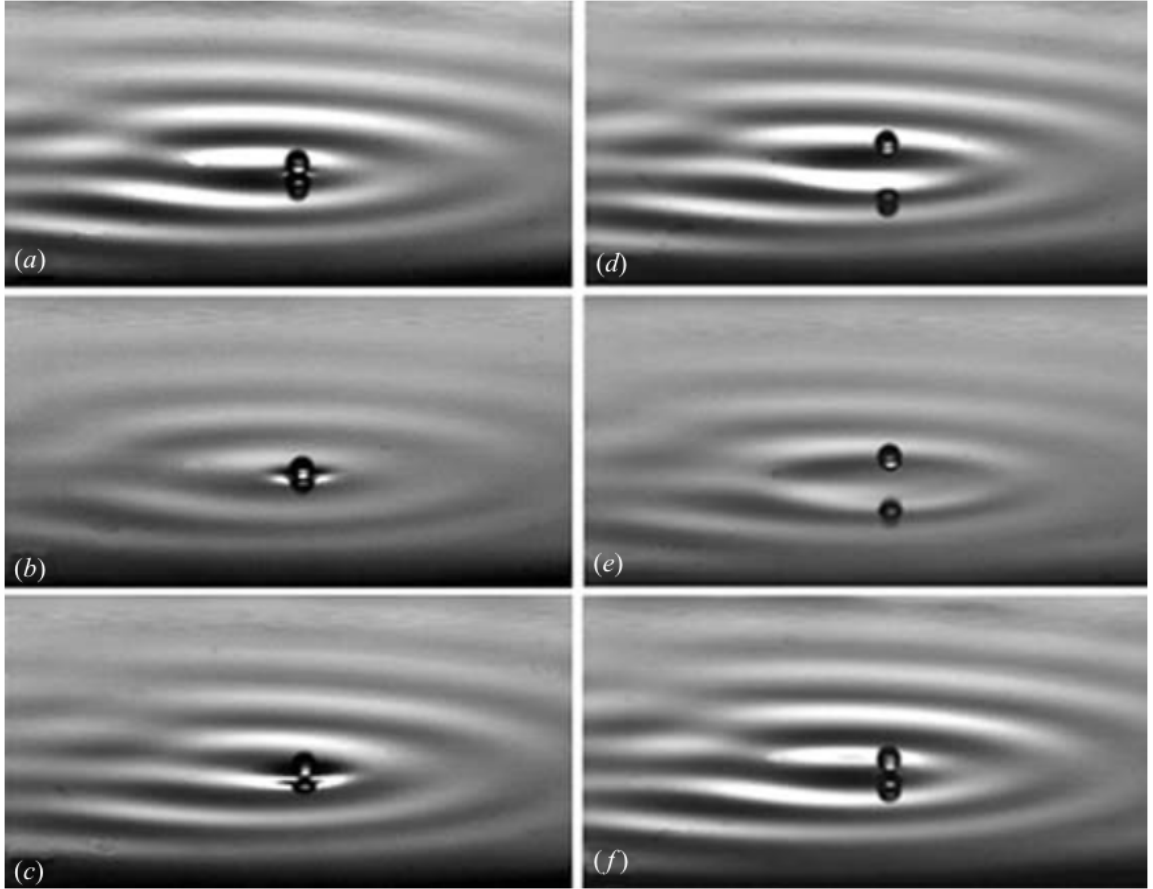


Figure 1.3: The series of pictures (a) - (f) show a walker during two forcing periods. The droplet bounces off of the slope of the localized wave, launching into the air, and then falls again on a new wave slope. This periodic process happens multiple times per second, giving the droplet the appearance of walking across the surface. Figure from [12]

Bound States

A periodic damped wave allows for two bouncers to form a **bound state**: a configuration in which the droplets remain a fixed distance apart [13]. Starting far away from one another, two droplets drift towards one another until a fixed distance d_0^{bd} . Increasing driving acceleration γ will decrease their separation distance d_0^{bd} (Fig. 1.4). These bound bouncers can form triangular lattices, though their periodicity is highly sensitive to the mass of the droplet. If the masses of the droplets differ, these configurations drift slowly and rotate because the waves produced by the larger droplet are larger creating an imbalanced wave field [14]. Finally, the droplets can bounce in phase with one another (they both land at the same time and reach their peaks at the same time) or completely out of phase with one another (as on lands, the other reaches its peak).

Walkers can also form bound states. Two walkers of the same size that are approaching one another can form an orbit around their center of mass as shown in

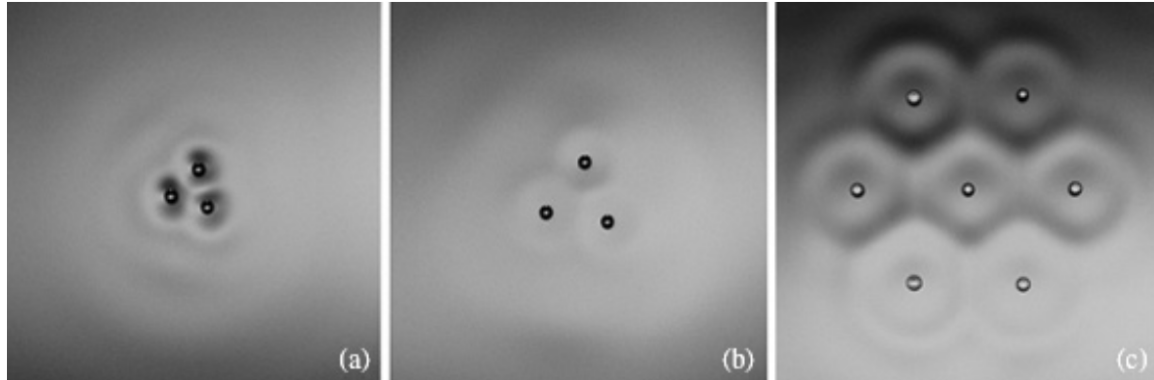


Figure 1.4: In (a), the trio of droplets organize themselves into a triangular lattice separated by distance d_0^{bd} . The forcing acceleration has been increased in (b), and the droplets are more spread out with a larger d_0^{bd} value. Bound states can include a large number of bouncing droplets, as demonstrated by the 7 bouncing droplets shown in (c). Figure from [13]

Fig. 1.5. Between the two droplets is the fixed distance d_n^{orb} given by

$$d_n^{orb} = (n - \epsilon_0)\lambda_F \quad (1.5)$$

where λ_F is the wavelength of the localized Faraday waves estimated by Eq. (1.1), ϵ_0 is a fixed distance which is the same for all orbitals of these walkers (usually in the range $0.15 < \epsilon_0 < 0.25$ depending on droplet diameter), and $n = 1, 2, 3, \dots$ for drops that are in phase or $n = 1/2, 3/2, 5/2, \dots$ for drops out of phase. Orbiting periods are approximately proportional to d_n^{orb} , which ends up meaning that the velocity of the orbiting walkers is a little less than the velocity of a free walker [12]. Droplets of equal mass will orbit around their center of mass, which ends up being in the middle of their orbit. Droplets of differing masses will still orbit around their center of mass, which will be closer to the larger mass than the smaller mass.

Scattering States

Two identical walkers headed towards each other can form fixed orbits, or they can scatter. **Scattering** describes an interaction in which droplets are deflected through their wave fields, and never actually make contact with one another. Most of the interactions of a walker are scattering of some form. For example, if a single walker approaches the wall of the tray, it will never actually touch the wall. Instead, the guiding wave reflects off of the wall and modifies the wave field such the droplet will scatter in the opposite direction.

1.1.4 Path Memory

Path memory is a parameter that can be varied in this setup; essentially it captures the importance of damping in the system [15]. Every time the droplet impacts the bath, it creates a radial traveling wave. Over the course of many bounces, a guiding

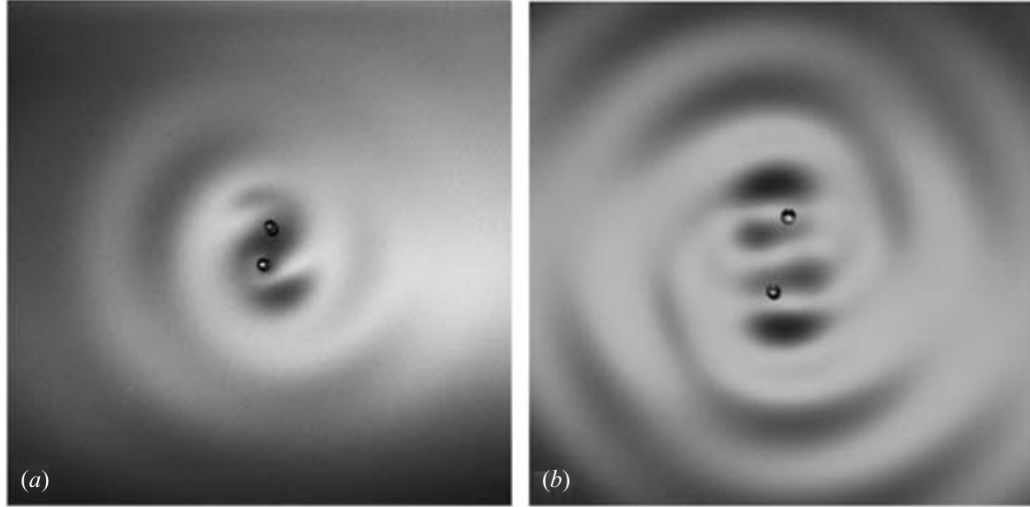


Figure 1.5: The figures show two droplets of equal size orbiting their center of mass. In (a) the droplets bounce out of phase with $n = 0.5$ and $d_n^{orb} = 1.65$ mm whereas in (b) the droplets bounce in phase with $n = 1$ and $d_n^{orb} = 3.7$ mm. Figure adapted from [12]

wave field composed of a superposition of the many waves arises. In this way the wave field ‘remembers’ previous interactions, but is at the same time being periodically ‘updated’ with every new bounce of the droplet. Because droplet motion is influenced by the wave field, controlling the damping of the wave field will influence the path of the walker.

For a bouncing droplet in which the guiding waves decay relatively quickly, the droplet can only be influenced by relatively recent waves. This kind of behavior is characterized as a low memory. Conversely, a high memory system is one in which waves do not decay quickly; they propagate outwards and reflect off of the surfaces of the tray before reflecting back and interfering with the other waves produced by the droplet. As one gets closer to the Faraday threshold, one achieves higher and higher memory because waves last for longer. The quantum-like features of this experiment arise in the high-memory limit.

The non-dimensional memory parameter is formally defined as:

$$M_e = \frac{T_d}{T_F(1 - \gamma/\gamma_F)},$$

where T_d is the decay time of waves in the absence of vibration and T_F is the period of the Faraday waves ($T_F = 1/f_F$) [16]. It will suffice to discuss memory as a fraction of the Faraday threshold γ/γ_F , since the fraction and M_e are monotonically related. As the value of γ/γ_F increases (we get closer to the Faraday threshold), M_e increases. Eventually as γ/γ_F approaches 1, the memory parameter approaches $+\infty$. Thus, higher forcing γ goes hand in hand with higher memory M_e .

In practice, walking arises above a value of $\gamma/\gamma_F = 0.94$, where as more quantum-like phenomena arise at values of $\gamma/\gamma_F = 0.97$ and above [17]. Deviations in memory

γ/γ_F as small as ± 0.01 can have drastic differences in both long term and short term droplet behaviors [16].

1.2 Droplet System as a Quantum Analog

Classical mechanics seeks to mathematically describe the motion of relatively large scale objects under action of forces. It was, until the late 19th century, physics. Physicists in the early 20th century, after a couple of very puzzling experiments, slowly began realizing that matter at the nanoscale behaved very differently than what they'd been studying in macroscale world. Quantum mechanics was developed, from the ground up, with the aim of mathematically describing this brave new world. As with any new behavior, a variety of theoretical explanations with mathematical foundations were tossed around, until the Copenhagen interpretation of quantum mechanics emerged from the 1927 Solvay conference. The Copenhagen interpretation was spearheaded by Niels Bohr and Werner Heisenberg, and it is a way of describing the strange experimental results. In the modern day, physicists teach and preach the Copenhagen interpretation of quantum mechanics because it is in excellent agreement with experiment; it is more developed than any other the other interpretations; it is the lesser of two evils (locality/non-realism over non-locality/realism); it has not been disproven; and because, well, that's how they learned it.

The oil droplet system is the first known classical system that behaves *like* a quantum system. It exhibits a variety of the same counter-intuitive interactions also seen in quantum mechanics, when subject to experiment. These include single particle double slit diffraction [18], quantized orbits , tunneling (discussed below) [7], and others [11]. These unique features stem from the **particle-wave duality** that is central in quantum mechanics: the idea that a particle can behave like a particle in some circumstances and like a wave in other circumstances. In the pilot-wave hydrodynamic system, the this is represented by the walker which is both a droplet and a wave.

The astute reader will point out that the oil droplet system is slightly different since the walker is a droplet *and* a wave, while the Copenhagen interpretation describes an electron (for example) as a particle *or* a wave. That's because this the oil droplet system isn't analogous to the Copenhagen interpretation of quantum mechanics. It actually bears remarkable resemblance to a somewhat obscure theory proposed by L. de Broglie in 1924, the so-called “double solution” theory. De Broglie's ideas were half-baked, but the theory essentially described a pilot-wave that guides a particle, which is then goverened by a long term statistical wave. His theory was picked up and modified by David Bohm in 1952, where it lost it's relevance to this model. Perhaps it's time we picked it back up.

1.2.1 Tunneling

Tunneling in Quantum Mechanics

Tunneling is one of the phenomena that is unique to the quantum world. At the classical level, we can take the example of a basketball thrown at a brick wall: the ball will hit the wall and bounce back every time we try it. When shift to the quantum scale, if we have a particle headed towards a barrier of a given potential energy, it will not necessarily bounce back. Depending on the characteristics of this potential, there will be a few times in which the particle will **tunnel** through the barrier, shooting out on the other side. It is not completely fair use the basketball-wall example as an analogy for the particle-barrier interaction because the “effective potential energy” of the brick wall is much higher, relatively, than that of the quantum potential barrier. For a high enough potential, the particle will also (almost) always bounce back. The point is that there really is no exact analogy in classical mechanics to tunneling at lower potentials for which tunneling is probabilistic.

Tunneling in the Bouncing Droplet System

A study performed by Eddi et al. examined tunneling in the bouncing droplet system [7]. In this setting, tunneling takes the form of the droplet tunneling through (or being reflected by) a subsurface barrier as depicted in Fig. 1.6. The droplet never actually travels through the barrier, since it bounces on the interface, but the analog to quantum tunneling remains, because as the droplet approaches the barrier it is affected by the region of a different “potential”.

For a different depth of fluid H , a tray will have a different γ_F . If a tray has various regions of different depths, then these different regions will behave slightly differently. This means that when a walker travels from an area of one depth to an area of another depth, it is entering an area in which its behavior will change. This effect can be seen when a walker is pushed back from a under-the-surface step, seemingly without any contact with the droplet. In certain cases, the walker will actually tunnel across the step; that is, it will continue to walk along the surface of the oil bath and pass into the new region of different depth, without reflection. Adjusting the width of the region as well as its depth will affect the behavior of the droplet. If we make this region of the tray of width e with depth h in a bath that otherwise has depth H , then we can think of it as a potential barrier. As the droplet steps over the barrier, it becomes a bouncer, with different dynamics. The unpredictability of the tunneling comes from the complex interaction between the drop and its guiding wave.

Eddi et al. built a rhombus shape which forced the walker across the center of a rhombus shown in Fig. 1.7 (a) - (b). A barrier was then placed across the diagonal of the rhombus, perpendicular to the direction of travel of the walker, so that the walker would run into the wall at a perpendicular angle. They discovered that by increasing the barrier width, the tunneling probability decreased. They also discovered that as γ/γ_F approached 1, they saw faster droplets which, they showed, had higher probabilities of tunneling (Fig. 1.7 (c)).

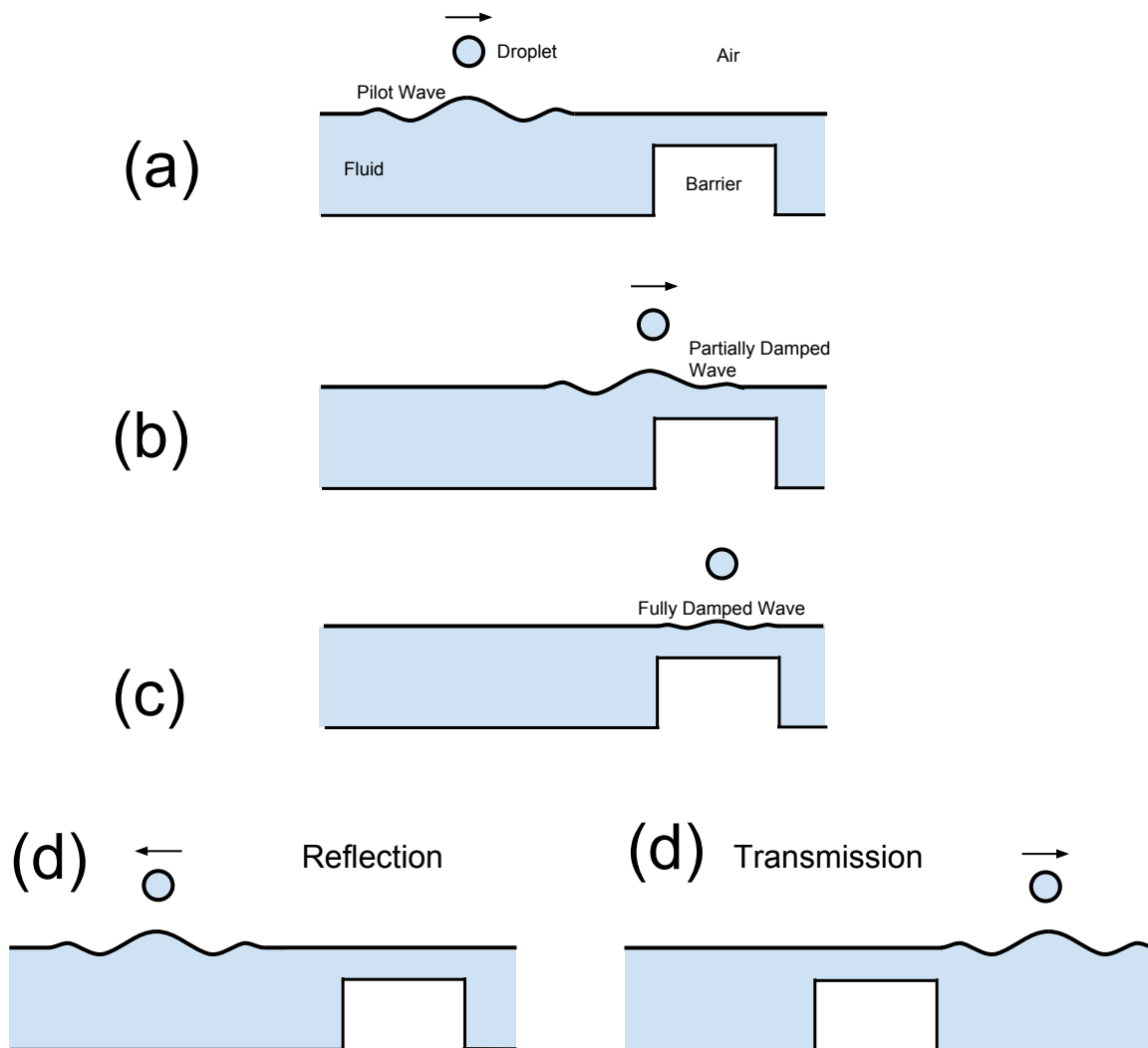


Figure 1.6: A diagram of the droplet-barrier interaction. In (a) the droplet moves towards the barrier. As it gets closer (b), the guiding wave is damped. In (c) the guiding wave is fully damped, and then the droplet will either reflect back from where it came (d), or carry on as shown in (e).

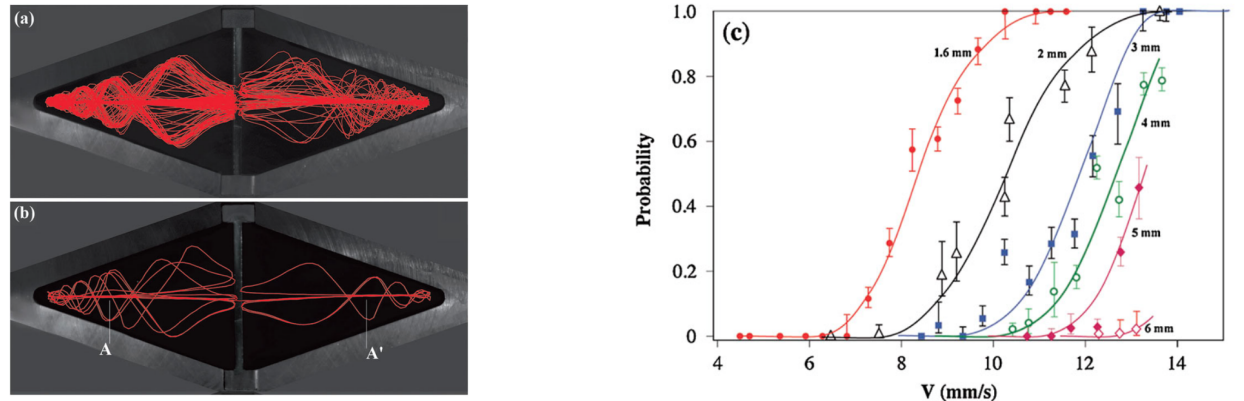


Figure 1.7: In (a) and (b) we see the path of a droplet traced out over many collision with the barrier in then rhombus shaped tray. The plot (c) shows the tunneling probability as a function of walker velocity. Figures from [7]

Chapter 2

Experimental Design

In the bouncing droplet system we observe a unique interaction between a droplet and its wave that showcases various novel behaviors under different circumstances. In the experiments discussed herein, we will look at how features *underneath* the surface of the oil (i.e. on the “floor” of the tray) affect the motion of the droplet.

A raised object on the floor of the tray (but still underneath the surface of the oil) can have an effect on height of the surface waves, and thus, on the motion of the walker [7]. Sometimes a droplet headed towards a raised object will be reflected backwards, as if from a collision with the object. For this reason, we refer to a raised object as a barrier.

Oftentimes however, the droplet slows down, but continues on and crosses the barrier without a collision. This is analogous to “transmission” in the quantum mechanical process of tunneling. For a given barrier of a certain height and width, there is a probability of tunneling unique to that barrier. Earlier studies have shown that increasing barrier width decreases probability of tunneling [7]. This study looks at how the height of the barrier affects the tunneling probability.

To test the effect of a barrier’s height on the probability of tunneling, I used a combination of procedures from the investigations of Bush et al. [11], Couder et al. [5], and specifically, Eddi et al. [7]. These were slightly modified to fit some of the unique features of my experiment. In this section, I aim to give some of the reasoning behind the design of the experimental apparatus and data collection techniques, both of which are not well described in the literature.

2.1 Setup

A schematic of the experimental setup is shown in Fig. 2.1, and a picture of the actual setup is shown in Fig. 2.3(a). A waveform generator creates a sinusoidal signal which is amplified and fed into a shaker. This signal drives the shaker, which vertically vibrates the tray containing the fluid. Both the frequency and the amplitude of the vertical oscillations can be controlled. An accelerometer records the vertical acceleration of the tray and is read using an oscilloscope. A camera records the droplet as it bounces along the surface of the oil.

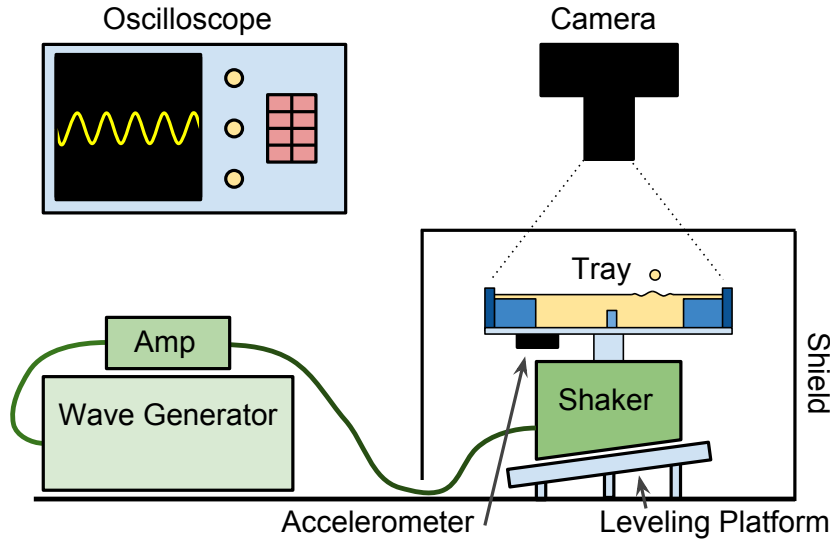


Figure 2.1: The experimental setup. The amplified signal from the wave generator drives the shaker, which shakes the oil-filled tray. The accelerometer generates a signal, which is read by the oscilloscope. The shield blocks disturbances to the experiment, while allowing the camera to document the trials.

2.2 Materials

The key components of this experiment are the shaker, the oil, and the tray. In this section I will describe the specifics of this holy trinity, as well as some of the additional components used in data collection.

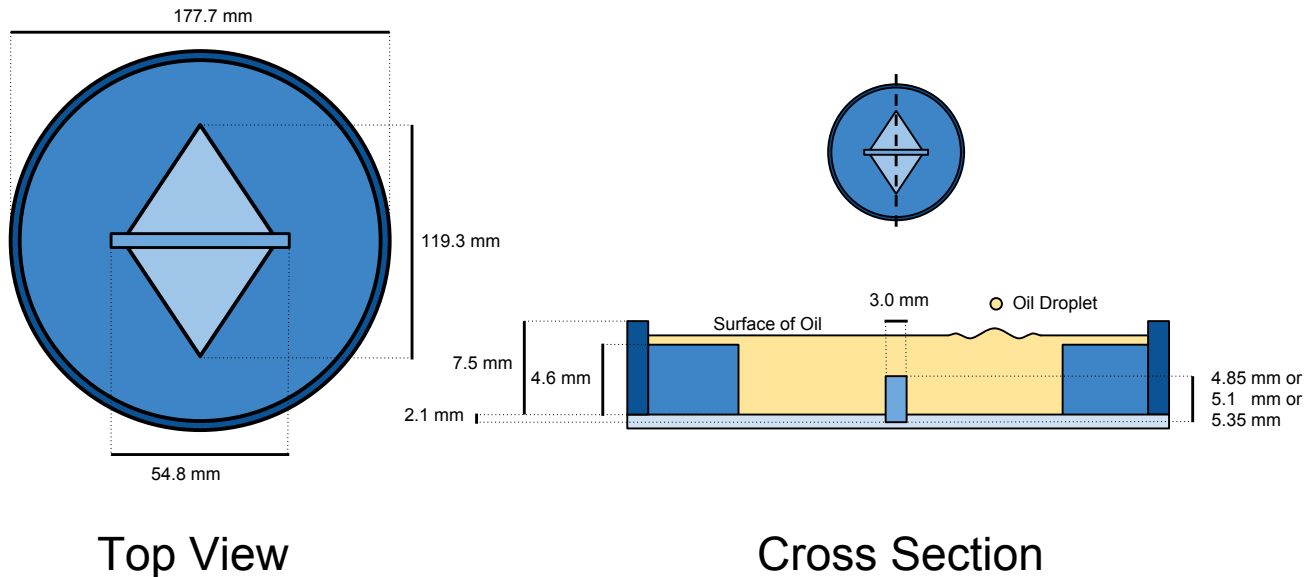
2.2.1 Tray

The tray was fabricated from acrylic plastic parts that were cut on the Trotek Rayjet 300 laser cutter in Reed's machine shop. The manufactured components were then glued together with Scigrip Weld-On 3 assembly adhesive. The tray's design, which was based off of the tray in the tunneling experiment of Eddi et al. [7], naturally guides the droplet into a perpendicular collision with the barrier. A detailed schematic of the tray is shown in Fig. 2.2.

A thin layer of oil spills over the constraining rhombus shape. As long as the layer is thin enough, the droplet will remain in the rhombus container, but the waves will continue to propagate unimpeded. This gives the waves time to decay, meaning that the droplet's motion is not affected by reflections of previous waves from the sidewalls, and is instead guided only by the unreflected waves.

The rhombus shape serves to steer the droplet into a perpendicular collision with the barrier. It does this by forcing the droplet to pin-ball into the acute corner of the rhombus and shoot out towards the barrier as shown in Fig. 2.3(c).

I designed my experiment to test barriers of three different heights: 2.75 mm, 3.0 mm, and 3.25 mm, measured from the bottom of the rhombus. A thin barrier of plastic made by the laser cutter has the tendency to bend and warp over time.



Top View

Cross Section

Figure 2.2: The specifications of the tray design. The top view (left) highlights the main elements in the tray, while the cross section (right) illustrates the topography of the tray. Depth is represented by the shading; darker shading is shallower.

To avoid this problem, we made the barriers taller than the specified heights. Then we created a cut-out in the bottom of the rhombus so the barriers could be inserted and held in place by the tight fit. The barrier cut-outs were deep enough to exactly counter the added height of the barrier, so the barriers still had (when measured from the surface of the rhombus) heights of 2.75 mm, 3.0 mm, and 3.25 mm. This design also solved the problem of fixing the barriers in place, while allowing them to be easily removed. The particular heights of the barriers were chosen because they allowed for both passage over and blockage by the barriers depending on the parameters. Other barriers that were too tall blocked all of the droplets (3.5 and 4.0 mm), while barriers that were too short (1.0 and 2.0 mm) did nothing to prevent the droplet from crossing over.

The bottom of the tray was painted black in order to improve contrast, allowing the droplet to be more easily tracked by eye and when using a camera.

2.2.2 Silicone Oil

Silicone oil was the ideal choice of fluid for this experiment because it remains clean, it has a low vapor pressure (so it does not evaporate), and it can be purchased in a range of specific viscosities. The silicone oil used in this experiment had a viscosity of 20 cSt (its viscosity is a little closer to water than olive oil) and was purchased from Clearco Products Co. Inc., Bensalem PA (CAS No: 63148-62-9). 20 cSt silicone oil, like the one used by Bush et al. [11] was chosen because it exhibits walking behavior over a wider range of parameters [11] than more viscous oil, such as the 50 cSt viscosity oil used by Couder [5]. Depending on the height of the barrier and the desired height of

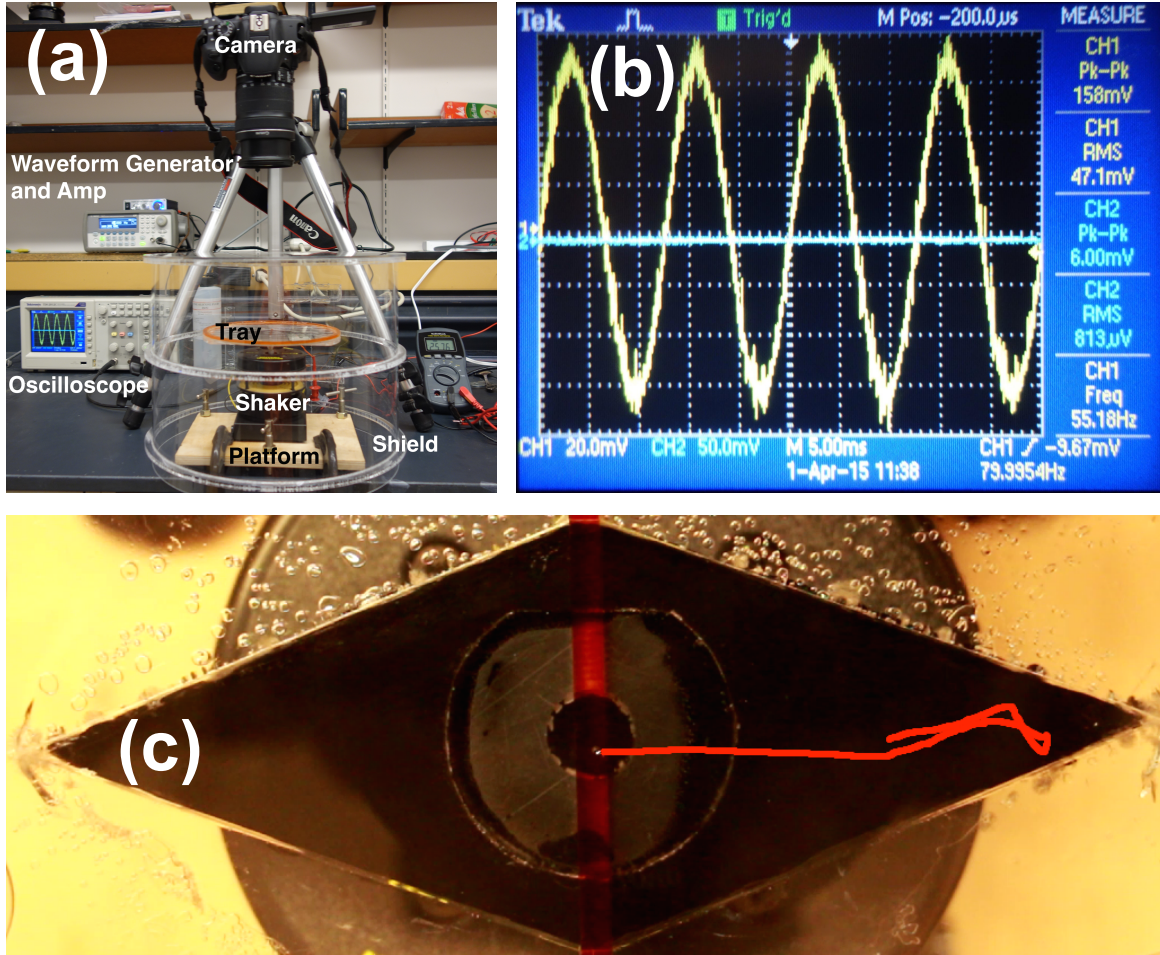


Figure 2.3: (a) The actual experimental setup. (b) The screen of the oscilloscope, showing the output from the accelerometer. The sine wave is proportional to the acceleration of the tray, and records a frequency 79.9954 Hz and a peak to peak voltage of 158 mV. (c) The path of a droplet of width 0.87 mm, highlighted in red, shows the droplet's motion as it walks into a corner before shooting out directly towards the barrier (orange).

oil above the barrier, the tray requires approximately 18.0 mL of fluid. This volume of oil left a different depth of oil above the barrier, depending on which barrier was in place. For the shortest barrier of 2.75 mm, the depth of the oil on top of the barrier was 1.5 mm. The intermediate barrier of height 3.0 mm had about 1.25 mm of fluid above it. The tallest barrier at 3.25 mm, only had 1.0 mm of fluid on top.

It was of vital importance to keep the oil as clean as possible since surface contamination leads to droplet coalescence. This meant protecting the oil from particulate matter that was already in the tray. Contamination was minimized by cleaning the tray before filling it and shielding it from the ambient dust using a plastic shield.

2.2.3 Shaker

To shake the tray, we used a mechanical wave driver made by Pasco Scientific, Roseville CA, model SF-9324. An acrylic component was attached to the bottom of the tray with a set screw, so that the tray was fastened to the thin rod that came on the shaker.

This shaker is designed to drive a string or an elastic cord, not a 200 gram tray with oil inside. In other words, the tray was probably at the limit of what the shaker was designed to handle. As a result, there was a notable decrease in performance after just a couple of minutes of vibration. The initial behavior could be partially recovered after an hour long rest, but after weeks of use there was a noticeable difference. This difference was apparent in the acceleration measurements made by the accelerometer; towards the end of a trial, a signal with a higher amplitude had to be generated to produce the same accelerations as from the beginning of the trial. For this reason, the shaker was replaced right before collecting the raw data and was allowed a resting period before beginning the following trial. The damping of the vibrations also meant that the acceleration signals from the accelerometer had to be continuously monitored, since the constant signal from the wave generator could not be trusted to produce a constant tray vibration.

2.2.4 Waveform Generator and Amplifier

The shaker was driven with an Agilent Arbitrary Waveform Generator model 33210. This was controlled digitally and was found to be more stable than other available frequency generators available in the Physics department (e.g. Tektronix CFG280). The waveform generator was usually set to produce a sine wave of 80 Hz. The signal from the waveform generator was amplified using a Lepai LP2020A+ digital amplifier. This allowed precise control of the the amplitude of the tray. The signal, which was also measured with a multimeter, was then fed into the shaker.

2.2.5 Accelerometer

As discussed in Chapter 1, knowing the tray's acceleration allows us to characterize the behavior of our system. To measure acceleration, we attached an ADXL 326 triple axis accelerometer (made by Adafruit, New York City NY) to the bottom of the tray using screws. This provided a much firmer hold than tape or glue while allowing for removal. The ADXL 326 has a range of $\pm 16g$, which is ideal for measuring the accelerations in our setup, which are usually below 5g's.

The signal from the z-axis of the accelerometer was measured directly on a Tektronix TDS 2012C oscilloscope. A sample output signal is shown in Fig. 2.3(b). For the vibrating tray, the output was approximately sinusoidal (as expected). The manufacturer's specifications for the accelerometer indicates a sensitivity of 57 ± 6 mV/g.

2.2.6 Shield

A large, see-through cylinder (covered at one end) was manufactured using the laser cutter. When placed over the tray, it served the purpose of keeping the oil clean from particulate matter and preventing air currents from influencing the motion of the walker.

2.2.7 Leveling Platform

A wooden leveling platform supported the shaker. Three adjustment screws allowed for precise adjustment of the tilt of the apparatus. The tray was tuned using a level placed inside the center of the tray (before the oil was added).

2.2.8 Camera

To document trials we used a Canon EOS Rebel T5i DSLR camera supported on a tripod and aimed directly down at the tray. Attached to the camera was a Canon 18-135 mm lens. Set in its Tv configuration (Time Value – allows for shutter control) and in video mode, the 18 megapixel image could be optically zoomed and manually focused on the bouncing droplet.

2.3 Procedure

Once the desired driving parameters were established (frequency and driving amplitude) so that walking behavior was observed, tunneling measurements at a few different barrier heights were made.

2.3.1 Finding the Walking Regime

Before investigating the rate of tunneling using different barriers, a rough estimate of the walking regime at a frequency of 80 Hz must be made. A “map” detailing the walking and bouncing threshold for different frequencies and amplitudes was produced. Reproducing this figure allows us to find the parameters that are specific to our unique setup, which could have slightly different height, tray, oil, and shaker configurations than those used in the literature.

Droplet size is measured using a recorded video of the walking droplet in motion. By comparing the number of pixels making up the diameter of the droplet, which is unknown, to the number of pixels making up the known length of the diagonal of the rhombus, we can estimate the length associated with each pixel, and thus find the diameter of the droplet in millimeters. For accurate droplet diameter measurements, a mean value composed of 9 separate droplet diameter measurements per trial was computed. The droplets had diameter on the order of 1.0 mm, as discussed in Section 1.1.

Driving acceleration values are measured by the accelerometer and displayed on the oscilloscope. To keep the acceleration constant across a measurement, the am-

plitude of the signal coming into the shaker was continuously adjusted in order to counteract the damping introduced as the shaker warmed up.

To ensure that every trial has the same oil depth, we measured the volume of oil (18.0 mL) before filling the tray using a 25 mL graduated cylinder with 0.5 mL graduation. Knowing the volume of the tray and of each barrier, we could calculate a value for the oil depth without interfering with the system. In this way, oil depth above the barrier (1.5 mm for the 2.75 mm barrier, 1.25 mm for the 3.0 mm barrier, 1.0 mm for the 3.25 mm barrier) could be made constant between trials.

2.3.2 The Experiment

This experiment utilized data collected from 3 independent trials. A trial consisted of measuring tunneling for three different barrier heights using a single droplet. At each height (and at a constant frequency of 80 Hz and constant tray acceleration), a string of continuous collisions were filmed with the camera. Between each measurement, the barriers had to be removed and replaced while the tray was still shaking in order to keep the droplet from coalescing. Since the size of the droplet changes its walking behavior, a constant droplet allowed for accurate comparisons between barrier heights. Not having a droplet of the same size is a major limitation to most of the research in the bouncing droplet system, such as in the other tunneling experiments [7], and the fact that we were able to keep ours constant is a great success. From this data, a basic tunneling probability was calculated, which provides the most simplistic analysis of this system.

The tray was designed such that most of the droplet's collisions with the barrier occur "head on" (i.e. perpendicular to the length of the barrier), but not all collisions unfold ideally. A more involved analysis using *Tracker* used the component of velocity of the droplet perpendicular to the length of the barrier to determine the probability of tunneling given this value. Since not all collisions in the simplistic analysis occurred at the same velocity, the perpendicular velocity method provided a more refined analysis of the phenomenon.

Chapter 3

Data Analysis and Results

3.1 Raw Data

The raw data consisted of a total of 7 videos and are laid out in Fig. 3.1. Barrier height, acceleration of the tray, Faraday threshold, and percentage of “transmissions” were recorded for each of the 7 videos. The 7 videos contained: one trial of a single droplet for all three barrier heights, another trial of a single droplet for all three barrier heights, and a final trial of a single droplet for the 3.0 mm barrier. The same droplet was used for each of the three barrier heights in a trial. There were between 12 to 24 separate collisions for each barrier.

| Trial | Recorded Data | From Tracker |
|---------|-------------------------------------|----------------------|
| Trial 1 | 2.75, γ , γ_F , %T, V | $3 \times D_1, v(t)$ |
| | 3.00, γ , γ_F , %T | $3 \times D_1, v(t)$ |
| | 3.25, γ , γ_F , %T | $3 \times D_1, v(t)$ |
| Trial 2 | 2.75, γ , γ_F , %T, V | $3 \times D_2, v(t)$ |
| | 3.00, γ , γ_F , %T | $3 \times D_2, v(t)$ |
| | 3.25, γ , γ_F , %T | $3 \times D_2, v(t)$ |
| Trial 3 | 3.00, γ , γ_F , %T, V | $9 \times D_3, v(t)$ |

Figure 3.1: For each barrier (2.75 mm, 3.0 mm, or 3.25 mm), the forcing acceleration (γ), the Faraday threshold acceleration (γ_F), and the percentage of “transmissions” (%T) were recorded. The oil volume (V) was recorded at the beginning of each trial. From *Tracker*, three measurements of the droplet diameter (D_n) were made along with the velocity of the droplet for every frame ($v(t)$).

These movies were then processed with *Tracker*. *Tracker* decomposes a video into multiple frames for the purpose of tracking an object in a video. By tracking the position of the object in every frame and knowing the time in between each frame ($\frac{1}{24}$ seconds), *Tracker* estimates the velocity of the droplet at every frame. We also want to know the size of each droplet, so we measure the diameter of the droplet using a function in *Tracker*. The diameter is measured multiple times in each movie, for

reasons explained in Section ??.

From the volume of the oil V and measurements taken of the tray, we can calculate the parameter h , which is defined as the height of the oil above the barrier. This was done by calculating the volume the “space” inside the tray, which required accurate measurements of the tray components.¹

3.2 Analysis

3.2.1 Tunneling vs. Oil Depth

Our primary interest in this investigation was determining how tunneling was affected by depth of oil. The results are shown in Fig. 3.2. The droplet never crossed near the value $h = 1.0$, whereas it always crossed at a value $h = 1.5$. In between, at a depth $h = 1.25$, we have both transmissions and reflections at a rate that changes for every trial. If we consider the droplet diameter, we see that the plot suggests that the transmission coefficient increases depending on the diameter of the droplet.

3.2.2 Tunneling by Droplet Velocity

Not every droplet barrier collision was ideal. Many times, the droplets approached at an angle or at different velocities which means that it is a little misleading to speak as if every collision was exactly the same. One way we can standardize collisions is by looking a perpendicular velocity at 5 mm from the center of the barrier, as shown in Fig. 3.3.

We expect the perpendicular component of velocity to be important because it proved critical in the study of barrier width carried out in ??, and because it’s intuitive: if the droplet moves faster, it has greater momentum and is more difficult to stop. Fig. 3.4 shows every collision for the middle barrier height, and the result of each interaction.

In trials 2 and 3, note that the majority of the droplets with the fastest perpendicular velocities are usually the ones that pass through the barrier, as expected. This does not seem to be the case for trial 1, for unknown reasons.

3.3 Sources of Error

With a system like this one, sensitive to every tweak in any parameter, it’s crucial to keep track of the errors so that we can consider the limitations these errors could have on our conclusions. Below I discuss the nature of the experimental errors associated with my measurements.

¹The function making this calculation can be found in the Appendix.

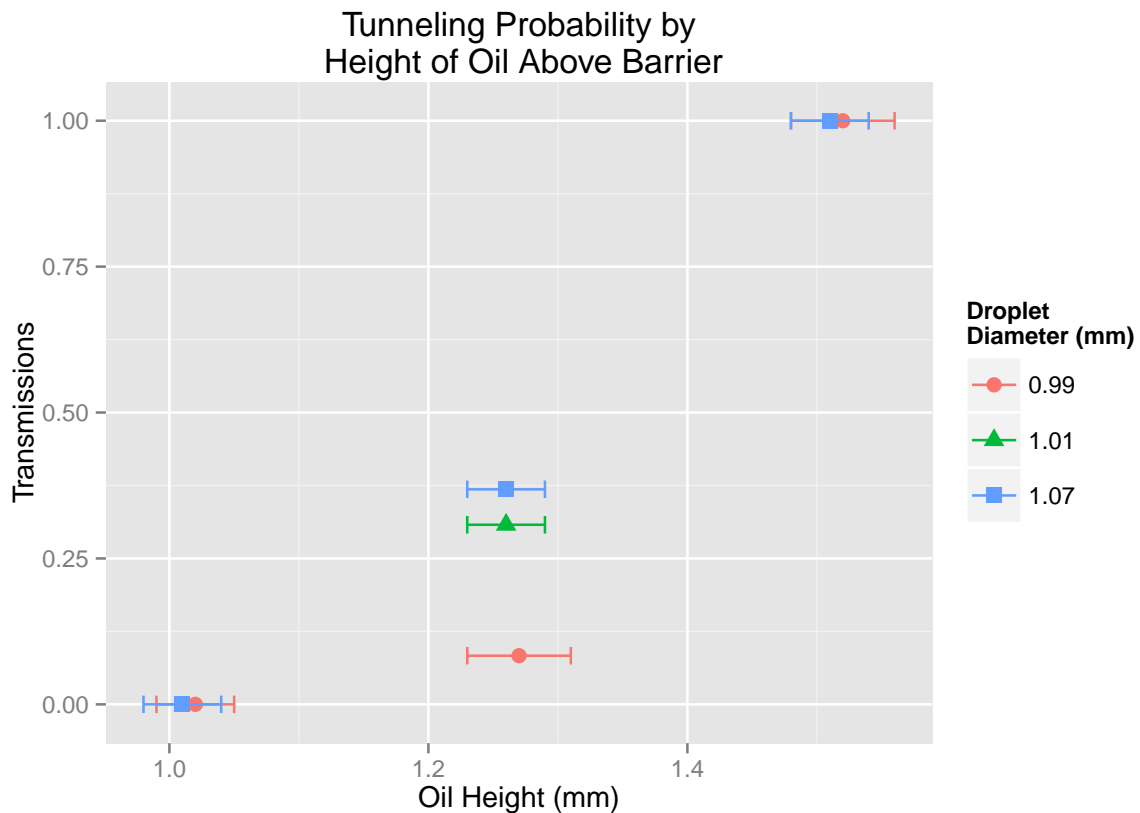


Figure 3.2: The proportion of transmissions for all collisions as a function of oil height above the barrier. Each color corresponds to a single trial for which the droplet was kept constant.

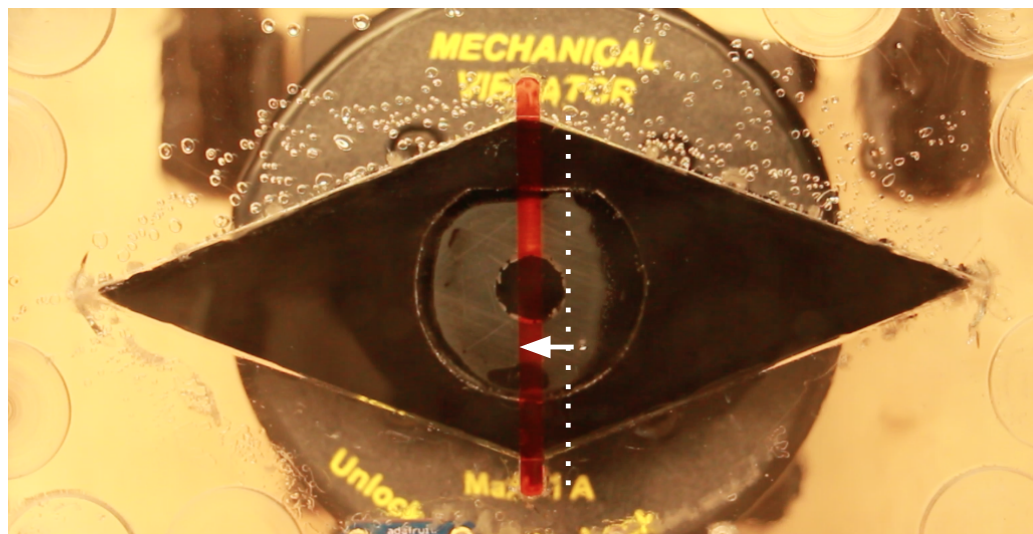


Figure 3.3: The image shows the point at which the perpendicular component of velocity was made, at 5 mm from the middle of the barrier.

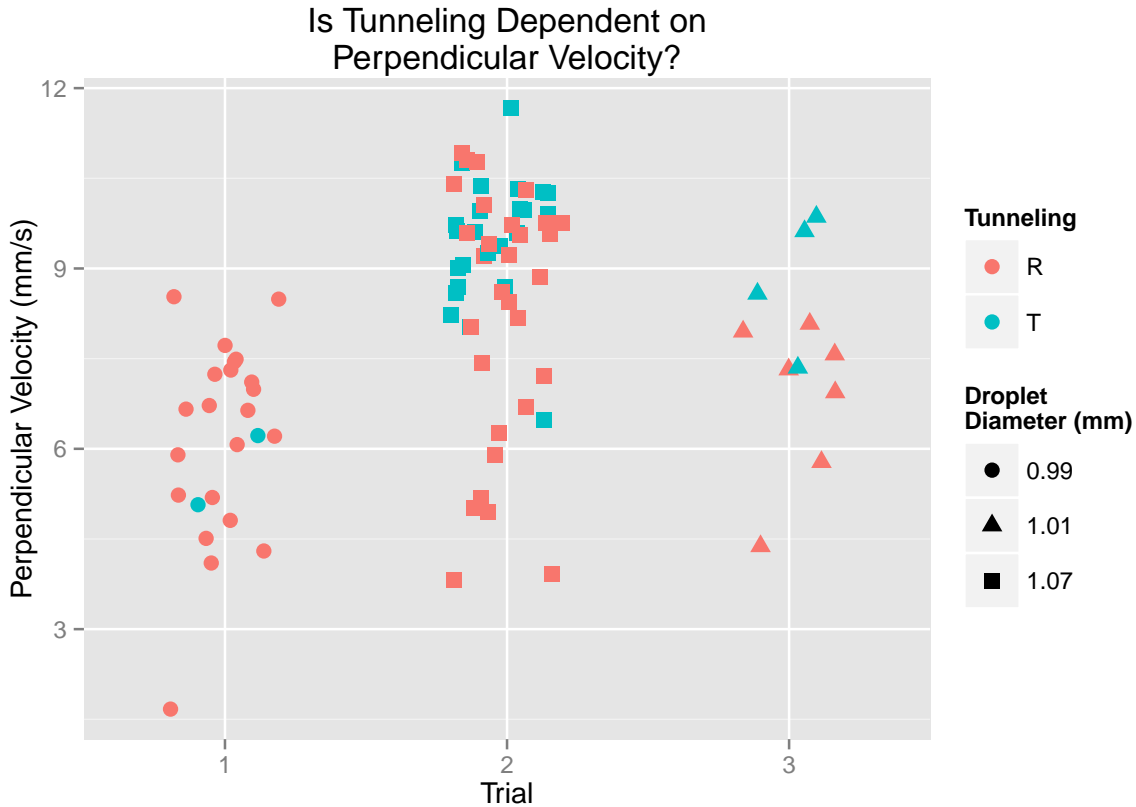


Figure 3.4: The result of each collision for the middle oil depth. The color represents the outcome of the collision (either transmission (T) or reflection (R)), and the shape represents the diameter of the droplet.

3.3.1 Droplet Diameter

The droplet diameter measurements were made using the *Tracker* program. Knowing the length (in mm) of another object in the frame, in this case the length of the rhombus cutout inside the tray, we can measure the length of anything else in the frame (in mm). This works by finding the length in mm associated with each pixel in the frame, then knowing the width in pixels of the droplet, we can calculate its length in mm.

$$\frac{\text{length of rhombus in mm}}{\text{length of rhombus pixels}} = \frac{\text{diameter of droplet in mm}}{\text{diameter of droplet in pixels}}$$

Since each has a defined length, and because we can't resolve anything within that pixel, our error is associated with that measurement is at least the width of a pixel, usually around **0.08 mm**. There is also an error associated with the initial measurement of the rhombus in pixels, since it can be difficult to discern where exactly each point lies.

Additionally, the droplet does not remain a perfect sphere as it bounces. At the bottom of its bounce, it will be squished and appear (from the top view) wider than

usual, where at the moment of lift it will be less wide (from the top) than usual. Since the camera recording our data shoots at 24 frames per second, it's impossible to know at what point in the bounce the droplet is, so it's impossible to know when to measure the diameter of the droplet. For this reason we measured the diameter of the droplet in 3 frames per at each of the 3 barrier heights, and with the total of 9 separate measurements we averaged the results.² Multiple measurements give us an associated standard error, which combined with the error due to pixel limitations, give us error bars.

Our measurement procedure helped reduce the error associated with the changing size during a bounce. It also reduced the error associated with finding the exact mm to pixel ratio because within each trial, each barrier height was tracked separately so a new mm to pixel ratio was formed.

3.3.2 Droplet Velocity

The droplet velocity was measured using *Tracker*. The error in this measurement can be attributed to the autotracker function, which automatically tracks the motion of the droplet using a built in algorithm. Autotracking is mostly spot on, but if left alone for a few thousand frames, the marker begins to drag behind. The error can be estimated to no more than 10 pixels, corresponding to $\pm 0.8 \text{ mm/s}$.

3.3.3 Height of Oil

The volume of oil was measured, before each trial, with a graduated cylinder marking every half milliliter. With measurements on the order of 18.0 mL, there was an associated error of $\pm 0.10 \text{ mL}$. Then, oil was lost between each barrier adjustment, since pliers were inserted in the oil to pull each barrier out, and a little bit of oil remained on the barrier and on the pliers each time. The volume of fluid lost after each barrier replacement was estimated to be about 3 droplets of diameter 3.0 mm. This corresponds to a loss of **0.014 mL** of oil after every change in barrier. Finally, the volume of the oil was used to estimate the height of the oil above the barrier. The elements in the tray were manufactured for this experiment, and were then measured using a device yielding an error of $\pm 0.03 \text{ mm}$.

For the height of the oil above the barrier, the above estimates provide us with an error on the order of about $\pm 0.35 \text{ mm}$. The amount of fluid lost after each barrier replacement corresponds to a height decrease of **0.36 mm** (for a barrier of the same size).

It's impossible to account for factors such as the amount of oil left in the graduated cylinder, or the oil that may have seeped into microscopic fractures inside the tray. We assume these systematic errors to remain relatively constant over the duration of the experiment. This means that the pattern of our results should remain about the same, even if the exact numbers are slightly off.

²For the third trial in which only one barrier was used, the mm to pixel ratio was re-fit after three diameter measurements, in order to mimic the procedure of the first two trials.

3.3.4 Consistency of Memory

The shaker's acceleration decayed the longer it ran which lead to changes in droplet behavior. This could be seen by the acceleration measured by the accelerometer, the acceleration decreased as the input signal remained constant. To counteract the changing acceleration, the amplitude of the signal was increased as such that it remained constant (as measured by the accelerometer) throughout the length of the experiment. After replacing each barrier, the Faraday threshold to that setup. As the amount of oil and the barrier height changed, the Faraday threshold also changed, so keeping the same input signal was not an option. Rather, in all experiments the *memory* was kept constant, at around 98% of the Faraday frequency. Because at different memories we see different droplet behaviors, a constant memory meant we could keep the behavior the same in all trials.

3.3.5 Imperfect Droplet Motion

The intent of the tray design was to create droplet trajectories such that their collisions were perpendicular to the length of the barrier. However, in practice, this was not the case. Trajectories tended to deviate to one side and impacted the barriers at an angle. Often, in situations in which the droplet was reflected, the trajectory would become a small limit cycle that would repeat for a couple of periods before diverging off in another path.

The perpendicular velocity measurements were a work-around since they provide a more descriptive picture of each interaction. Even with this crutch though, the angled trajectories are a symptom of an imperfect setup. Though great care was taken to ensure that the tray was flat, it was impossible to adjust the mostly vertical direction of vibration to be perfectly vertical. When the oscillations are not exactly vertical, the oil inside the tray does not shake evenly, which leads to imperfect droplet motion. Rather than moving in a straight line until encountering a barrier of some sort, the droplet will slowly curl away from certain areas within the tray. Additionally, the tray in our setup was attached at a single point by a rod connected to the shaker. This could have lead to bending of the acrylic at the edges, since the tray was so big. A mechanical shaker, as detailed in [19], would provide a much better base than the smaller shaker used in this experiment. It also has the added benefit of shaking the entire tray at once, rather than just a single point. While the error due to this component cannot be measured numerically, it should be considered when drawing conclusions.

Conclusion

Here's a conclusion, demonstrating the use of all that manual incrementing and table of contents adding that has to happen if you use the starred form of the chapter command. The deal is, the chapter command in L^AT_EX does a lot of things: it increments the chapter counter, it resets the section counter to zero, it puts the name of the chapter into the table of contents and the running headers, and probably some other stuff.

So, if you remove all that stuff because you don't like it to say "Chapter 4: Conclusion", then you have to manually add all the things L^AT_EX would normally do for you. Maybe someday we'll write a new chapter macro that doesn't add "Chapter X" to the beginning of every chapter title.

4.1 More info

And here's some other random info: the first paragraph after a chapter title or section head *shouldn't* be indented, because indents are to tell the reader that you're starting a new paragraph. Since that's obvious after a chapter or section title, proper typesetting doesn't add an indent there.

Appendix A

The First Appendix

An appendix full of awesome

Appendix B

The Second Appendix, for Fun

An appendix full of win

References

- [1] Y. Couder, S. Protiere, E. Fort, and A. Boudaoud, “Dynamical phenomena: Walking and orbiting droplets,” *Nature*, vol. 437, pp. 208–208, Sep 2005.
- [2] D. Bohm, “A suggested interpretation of the quantum theory in terms of ‘hidden variables’ i,” *Phys. Rev.*, vol. 85, pp. 166–179, Jan 1952.
- [3] D. Bohm, “A suggested interpretation of the quantum theory in terms of ‘hidden variables’ ii,” *Phys. Rev.*, vol. 85, pp. 180–193, Jan 1952.
- [4] J. Walker, “The amateur scientist,” *Scientific American*, vol. 238, pp. 151–158, Jun 1978.
- [5] Y. Couder, E. Fort, C.-H. Gautier, and A. Boudaoud, “From bouncing to floating: Noncoalescence of drops on a fluid bath,” *Physical Review Letters*, vol. 94, May 2005.
- [6] M. Faraday *Phil. Trans. R. Soc. Lond.*, vol. 121, pp. 319–340, 1831.
- [7] A. Eddi, E. Fort, F. Moisy, and Y. Couder, “Unpredictable tunneling of a classical wave-particle association,” *Phys. Rev. Lett.*, vol. 102, no. 240401, 2009.
- [8] K. Kumar, “Linear theory of faraday instability in viscous liquids,” *Proceedings of the Royal Society A: Mathematical, Physical and Engineering Sciences*, vol. 452, pp. 1113–1126, May 1996.
- [9] J. Moláček and J. W. M. Bush, “Drops walking on a vibrating bath: towards a hydrodynamic pilot-wave theory,” *J. Fluid Mech.*, vol. 727, pp. 612–647, Jun 2013.
- [10] L. Rayleigh, “On the capillary phenomena of jets,” *Proc. R. Soc. Lond.*, vol. 29, p. 71, 1879.
- [11] J. M. W. Bush, “Pilot-wave hydrodynamics,” *Annu. Rev. Fluid Mech.*, vol. 47, pp. 269–292, 2015.
- [12] S. Protiere, A. Boudard, and Y. Couder, “Particle-wave association on a fluid interface,” *J. Fluid Mech.*, vol. 554, p. 85, Apr 2006.
- [13] S. Protiere, Y. Couder, E. Fort, and A. Boudaoud, “The self-organization of capillary wave sources,” *J. Phys.: Condens. Matter*, vol. 17, Oct 2005.

- [14] A. Eddi, D. Terwagne, E. Fort, and Y. Couder, “Wave propelled ratchets and drifting rafts,” *EPL (Europhysics Letters)*, vol. 82, p. 44001, May 2008.
- [15] A. Eddi, E. Sultan, J. Moukhtar, E. Fort, M. Rossi, and Y. Couder, “Information stored in faraday waves: the origin of a path memory,” *J. Fluid Mech.*, vol. 674, pp. 433–463, Mar 2011.
- [16] D. M. Harris and J. W. M. Bush, “Droplets walking in a rotating frame: from quantized orbits to multimodal statistics,” *J. Fluid Mech.*, vol. 739, pp. 444–464, Dec 2013.
- [17] A. U. Oza, D. M. Harris, R. R. Rosales, and J. W. M. Bush, “Pilot-wave dynamics in a rotating frame: on the emergence of orbital quantization,” *J. Fluid Mech.*, vol. 744, pp. 404–429, Mar 2014.
- [18] Y. Couder and E. Fort, “Single-particle diffraction and interference at a macroscopic scale,” *Phys. Rev. Lett.*, vol. 97, no. 154101, 2006.
- [19] D. M. Harris and J. W. Bush, “Generating uniaxial vibration with an electrodynamic shaker and external air bearing,” *Journal of Sound and Vibration*, vol. 334, pp. 255–269, Jan 2015.